Theor Chem Acc (2005) 114: 60–67
DOI 10.1007/s00214-005-0644-1

REGULAR ARTICLE

C. Kolczewski · K. Hermann

Ab initio DFT studies of oxygen K edge NEXAFS spectra for the $V_2O_3(0001)$ surface

Received: 10 September 2004 / Accepted: 17 December 2004 / Published Online: 8 July 2005

Abstract Theoretical near edge X-ray absorption fine structure (NEXAFS) spectra describing oxygen 1s core excitation have been evaluated for the differently coordinated oxygen species appearing near the $V_2O_3(0001)$ surface with half metal layer V′OV termination. Adsorption of oxygen above vanadium centers of the V′OV terminated surface (O_tV′O termination) results in very strongly bound vanadyl oxygen, which has also been considered for core excitation in this study. The angle-resolved spectra are based on electronic structure calculations using ab initio density functional theory (DFT) together with model clusters. Experimental NEXAFS spectra for $V_2O_3(0001)$ show a rather strong dependence of peak positions and relative intensities on the photon polarization direction. This dependence is well described by the present theoretical spectra and allows us to assign spectral details in the experiment to specific O 1s core excitations where final state orbitals are determined by the local binding environments of the differently coordinated oxygen centers. As a result, a combination of the present theoretical spectra with experimental NEXAFS data enables an identification of differently coordinated surface oxygen species at the $V_2O_3(0001)$ surface.

Keywords Vanadium sesquioxide · $V_2O_3(0001)$ surface · Surface termination · NEXAFS spectroscopy · Electronic structure · DFT · Cluster models

1 Introduction

Vanadium oxides form a large family of transition metal oxides where the formal oxidation state of the metal species ranges from +2 to +5. This is combined with a variety of exciting physical properties, e.g. structural, electronic, and magnetic phase transitions [1,2]. In addition, vanadium oxides are used as important components in catalysts for many chemical reactions of industrial importance [3–6]. In this study, we focus on vanadium sesquioxide, V_2O_3, where vanadium is in its formal oxidation state +3. This compound is a product of deep reduction of vanadium pentoxide, V_2O_5, in many catalytic processes. It undergoes a phase transition at 150–170 K from an anti-ferromagnetic semiconductor with monoclinic crystal structure below to a paramagnetic metal with rhombohedral corundum structure above the transition temperature [7].

While bulk properties of V_2O_3 have been studied extensively both by experiment and theoretically [8–11] well-characterized single crystal surfaces of the corundum structure have been investigated only for two surface orientations, (0001) and (10–12), in greater detail [12–14]. The hexagonal (0001) surface, which seems to be more easily accessible by experiment [14], allows for three intrinsic bulk terminations, OVV′, VV′O, and V′OV (denoted by the element composition of the three topmost atom layers, see below). So far, the most stable termination has not been identified by experiment. However, detailed LEED analyses and other studies of the atomic geometry at the (0001) surface of corundum type Cr_2O_3 [15–17] reveal a half metal layer termination with major relaxation of the topmost metal layer. This may suggest that the V_2O_3 (0001) single crystal surface exhibits a very similar surface structure, which has been confirmed by theory [18].

Recently, Dupuis et al. [19] studied thin $V_2O_3(0001)$ films on W(110) and Au(111) with several spectroscopic methods, such as X-ray photoemission (XPS), electron energy loss (HREELS), and near edge X-ray absorption fine structure (NEXAFS) spectroscopy. Their results indicate that exposure of the V_2O_3 surface to oxygen leads to surface vanadyl groups where the vanadyl oxygen may be removed by electron bombardment. This is consistent with the assumption of a half metal layer (V′OV) terminated $V_2O_3(0001)$ surface where the metal species of the topmost layer can be covered by adsorbed oxygen forming surface vanadyl species.

C. Kolczewski (✉) · K. Hermann
Fritz-Haber-Institut der Max-Planck-Gesellschaft,
Faradayweg 4-6,
D-14195 Berlin, Germany and Sfb 546
"Transition Metal Oxide Aggregates".
E-mail: kolczew@fhi-berlin.mpg.de

The corresponding termination will be denoted $O_tV'O$ in the following.

The $V_2O_3(0001)$ surface can contain differently coordinated oxygen depending on its termination and reconstruction. As an example, the intrinsic bulk termination V′OV leads to both three- and four-fold coordinated oxygen species near the surface. Further, the above mentioned $O_tV'O$ termination, suggested by experiment [19], contains also singly coordinated vanadyl oxygen. In all cases, changed coordination is expected to lead to different chemical behavior of the oxygen species. Therefore, it is important to study their electronic properties as a function of local coordination. This may also help the interpretation of experimental data from various spectroscopies, such as NEXAFS, allowing a discrimination of differently coordinated oxygen based on experimental information.

In this work, we use ab initio density functional theory (DFT) together with cluster models to evaluate the electronic structure of local environments at the $V_2O_3(0001)$ surface where we focus on the intrinsic V′OV and the experimentally suggested "chemical" termination $O_tV'O$. The electronic structure then serves as a basis to calculate angle-resolved NEXAFS spectra for 1s core excitation of differently coordinated oxygen near the $V_2O_3(0001)$ surface. The theoretical data can be compared with recent experimental NEXAFS spectra and explain spectral details by binding properties of the excited electron states near the differently coordinated oxygen centers.

In Sect. 2, we describe computational details of the present work while in Sect. 3 we present results of the calculations together with a detailed comparison with experimental angle-resolved NEXAFS spectra of the V_2O_3 (0001) surface [19]. Finally, in Sect. 4, we summarize our results and conclusions.

2 Computational details

Vanadium sesquoxide, V_2O_3, is described below $T_s = 150$–$170\,K$ by a monoclinic (distorted corundum) crystal lattice with lattice constants $a = 7.26\,Å$, $b = 5.00\,Å$, $c = 5.55\,Å$, and the angle $\beta = 96.75^\circ$ [20,21] where the elementary cell contains 20 atoms (four element units). Above the transition temperature T_s, a phase transition to the rhombohedral corundum structure is observed. The corresponding lattice constants and angles are $a = b = c = 5.46\,Å$ and $\alpha = 53.75^\circ$ [22,23] and the elementary cell includes two element units, i. e. ten atoms. Bulk crystals of both lattice structures contain vanadium in sixfold octahedral and oxygen in fourfold tetrahedral coordination (see Fig. 1a). Apart from a doubling of the elementary cell size, there are only very small structural differences between the two V_2O_3 crystal lattices. Therefore, in the present study we focus on the rhombohedral corundum structure, which is of higher symmetry than the monoclinic crystal structure. Possible differences in our results are not expected to be of relevance.

The rhombohedral V_2O_3 bulk is described along its (0001) direction by stacking alternating hexagonal netplanes of vanadium (two very close planes, V and V′) and oxygen (one plane O) in the sequence ...OVV′OVV′..., where the atom density of the oxygen netplanes is three times that of the vanadium planes [24]. This allows three intrinsic bulk terminations of the (0001) surface where we focus on the experimentally suggested [19] half metal layer termination, denoted V′OV, with only one of the two vanadium layers (V′) being topmost. The V_2O_3 substrate near this surface contains vanadium with three and sixfold as well as oxygen with three and fourfold coordination (see Fig. 1b, c). The above mentioned $O_tV'O$ termination of the $V_2O_3(0001)$ surface after oxygen exposure derives from the V′OV termination where each vanadium of the topmost layer is covered by an adsorbed oxygen forming a vanadyl group. Thus, the $O_tV'O$ terminated surface contains in addition singly coordinated oxygen.

Local sections of the V′OV terminated $V_2O_3(0001)$ surface are modeled by clusters of finite size reflecting the unrelaxed bulk geometry and containing up to 11 vanadium and 33 oxygen centers as sketched in Fig. 1b, c. The $V_{11}O_{33}$ cluster has been applied in previous theoretical studies [18,25, 26] of $V_2O_3(0001)$ surface properties, where dangling bonds of the peripheral oxygen centers were saturated by hydrogen, resulting in a $V_{11}O_{33}H_{33}$ model cluster. This saturation is not included in the present study dealing with electronic properties of oxygen close to the cluster center. Extensive test calculations have shown that the electronic structure of these oxygens of the inner cluster region is affected only very little by the presence of dangling bonds at the cluster periphery. Since the V′OV terminated $V_{11}O_{33}$ surface cluster contains three V′ atoms of the topmost layer, the $O_tV'O$ termination can be represented by a $V_{11}O_{36}$ cluster with three vanadyl groups. Here, the vanadyl V–O distance of $1.586\,Å$ is taken from previous geometry optimizations [26].

The electronic structure of the present clusters is calculated by ab initio DFT methods (program code StoBe [27]) using generalized gradient corrected functionals according to Perdew, Burke, and Ernzerhof (RPBE) [28,29] to approximate electron exchange and correlation. The Kohn-Sham orbitals are described by linear combinations of atomic orbitals (LCAO's), using extended basis sets of contracted Gaussians from atom optimizations [30,31]. The molecular basis sets used in the ground state calculations are all-electron double zeta plus valence polarization (DZVP) type for vanadium and oxygen, described by [5s3p2d] and [3s2p1d], respectively. The V basis is also used in the calculations of O 1s core excitation while for oxygen different basis sets are applied. The basis set at the oxygen center where the excitation initiates is IGLO-III [32] described by [7s6p2d] in order to obtain an adequate description of inner shell relaxation effects. The other oxygen centers in the cluster are accounted for by effective core potentials (ECP) including 1s electrons and [3s3p1d] valence basis sets [33] to avoid explicit mixing of 1s orbitals of the different oxygen centers. This approximation is found to result in faster convergence of the electronic structure introducing only negligible effects on the computed excitation spectra [34].

The calculation of O 1s core level excitation spectra for the clusters is performed within Slater's transition state

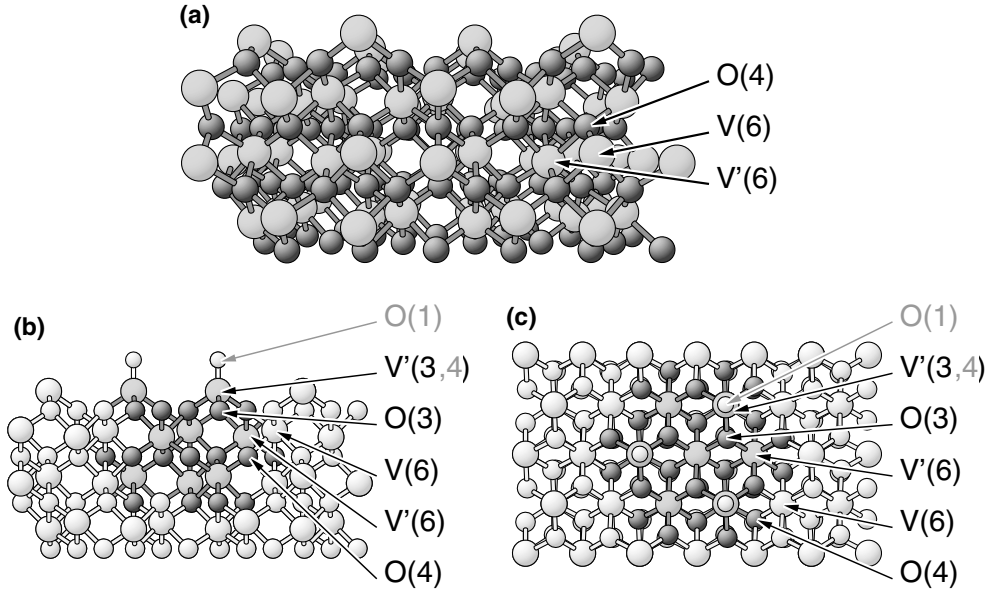

Fig. 1 **a** Crystal structure of rhombohedral V_2O_3 with netplane stacking along (0001). Oxygen centers (fourfold coordinated O(4)) are shown as small dark balls, vanadium centers (sixfold coordinated V(6), V′(6)) as large light balls. **b** Side view of the V′OV terminated V_2O_3(0001) surface with oxygen and vanadium centers labeled by their coordination. The additional vanadyl oxygen O(1) refers to the O_tV′O termination. The darker region at the surface sketches the $V_{11}O_{33}$ cluster used in the present calculations. **c** *Top view* of the surface shown in **b**

approach [35,36] in combination with a double basis set technique [37]. This approach starts from a self-consistent transition state calculation with a partially occupied O 1s core orbital at the ionization site (n_{O1s}=0.5 according to Slater [35, 36]). In a second step, the basis set at the excitation site is augmented by very diffuse [19s19p19d] functions and the electronic structure is re-evaluated non-iteratively, yielding all unoccupied valence orbitals and including approximate orbitals for energies above then ionization threshold. The resulting orbital energies and corresponding dipole transition matrix elements (determining absorption intensities) are then used to compute the angle resolved core level excitation (NEXAFS) spectrum by Gaussian convolution with varying broadening. A broadening of 0.5 eV is applied below the ionization threshold while within 10 eV above the threshold the broadening is increased linearly to 2.5 eV and kept fixed at this value for higher energies [38]. For further details see also [39–41].

The $V_{11}O_{33}$ cluster possesses an odd number of electrons and its ground state is a doublet state. As a consequence, two different core holes exist, one for alpha and one for beta spin. Test calculations comparing both core holes have shown that the spin dependent NEXAFS spectra are very similar in shape and only shifted slightly in energy by about 0.4 eV. Thus, in the following we present only spectra of alpha spin orbital excitation.

In Slater's transition state approach, the electronic core hole relaxation is not fully accounted for. Therefore, we shift all excitation energies by a relaxation correction, which is determined from calculations of fully relaxed ionized states for each of the differently coordinated oxygen species amounting to a global shift of 1.8 – 1.9 eV to lower energies. Further, all spectra are shifted by 0.4 eV to higher energies to include relativistic corrections [42].

3 Results and discussion

3.1 Intrinsic half metal termination V′OV

As discussed above, the V′OV termination of the V_2O_3(0001) surface offers two different types of oxygen, threefold coordinated O(3) in the second and fourfold coordinated O(4) in the fifth surface layer (see Fig. 1b, c). As a result, core excitation involving both oxygen species has to be included in calculations of angle-resolved NEXAFS spectra. Figure 2 shows theoretical NEXAFS spectra obtained from the $V_{11}O_{33}$ cluster calculations for oxygen 1s excitation, where two incidence/polarization directions of the incoming photon beam are considered (reflecting scenarios of recent experimental angle-resolved NEXAFS spectra [19]). The first geometry corresponds to a polar beam angle of $\alpha = 70^\circ$ with respect to the surface normal (near grazing incidence) where the polarization vector points 20° away from the surface normal. The second, $\alpha = 0^\circ$, reflects incidence along the surface normal with the polarization vector being parallel to the surface. Figure 2 includes for both angles α the total theoretical O 1s excitation spectrum together with its O(3) and O(4) derived contributions. These spectra are compared in the figure with recent experimental oxygen K edge NEXAFS spectra [19] (top curve of each plot).

It should be noted that, as a consequence of the C_3 symmetry of the V_2O_3(0001) surface which is also present in the model cluster, the angle-resolved NEXAFS spectra depend

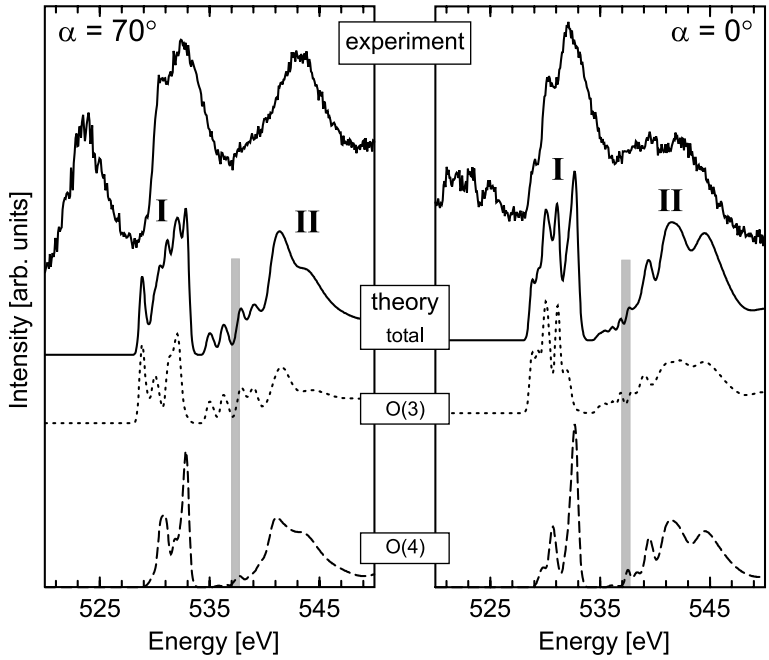

Fig. 2 Comparison of experimental angle resolved O K edge NEXAFS spectra with theoretical O 1s core excitation spectra for two different angles of photon beam incidence, $\alpha = 0°$, 70°, at the V′OV terminated $V_2O_3(0001)$ surface. For the evaluation of the experimental spectra, see text. The total theoretical spectra are decomposed into contributions from differently coordinated oxygen, O(3) (*dotted*) and O(4) (*dashed*). The gray line indicates corresponding oxygen 1s ionization potentials

only on the polar angle α of the incident photon beam with respect to the surface normal but not on its azimuthal angle φ. This is accounted for in the calculations by averaging the excitation spectra of three symmetry-equivalent oxygen centers O(3) and O(4), respectively. Further, the experimental curves of Fig. 2 are obtained from differences of NEXAFS spectra for a given angle α measured by partial yield detection (PYD) and those recorded in sample current mode [19] where the PYD data are believed to be more strongly surface sensitive. Thus, the difference spectra are expected to reflect electronic core excitations predominantly from atom centers near the surface (for details see [19]).

The theoretical spectra of Fig. 2 exhibit, for both photon beam angles α, two sets of peaks below (set I) and above the ionization threshold (set II) referring to specific oxygen 1s core excitations. (The O 1s ionization threshold at 537 eV is sketched by gray lines in Fig. 2 where the line widths denote the range of ionization potential (IP) values, 0.7 eV, of the differently coordinated oxygen.) Detailed analyses of the final state orbitals (C. Kolczewski and K. Hermann, unpublished) corresponding to peaks of the two sets give a clear picture of their origins. All excitations of set I at about 530 eV can be characterized by electronic transitions from O 1s to final state orbitals described as weakly antibonding combinations of oxygen 2p and vanadium 3d contributions. Depending on the direction of the O 2p contribution, the antibonding character differs and distinguishes between the excitation energies. If the dominant O 2p function in the final state orbital points toward an adjacent vanadium center with its dominant 3d functions focused along the corresponding V–O axis, the antibonding effect is largest and leads to highest excitation energies. On the other hand, final state orbitals where the antibonding mixture contains O 2p and V 3d functions of adjacent centers trying to avoid each other result in the smallest antibonding effect and lowest excitation energies. Similar effects, also due to the crystal-field split metal d components have been observed for adsorbate systems, e.g. for water on Pt(111) [43]. The excitations of set II at about 543 eV, i.e. above the ionization threshold, can be characterized by electronic transitions from O 1s to O 3p orbitals, where, as before, the direction of the 3p functions together with the geometry of the local binding environment discriminates between the different excitations.

The total theoretical spectra are decomposed in Fig. 2 into atom-derived contributions due to threefold and fourfold coordinated oxygen O(3) (dotted curves) and O(4) (dashed curves), respectively. This reveals sizeable differences between the two oxygen species. First, the energy ranges of both peak sets are larger for O(3) than for O(4) excitation, and peak set I for O(3) is shifted to lower energies with respect to that for O(4). Second, the intensity distributions within peak set I differ between the two oxygen species. Clearly, these differences originate from details of the local binding environment of the two types of oxygen which manifests itself also in the excited final state orbitals, determining the excitation spectrum by their excitation energies ε and by corresponding dipole transition matrix elements m. However, the local binding of O(3) with its three vanadium neighbors in a quasi-planar geometry and of O(4) with its four vanadium neighbors in a distorted tetrahedral arrangement is quite

complex. Therefore, simple geometric arguments are not adequate to characterize the differences between the two atom-derived spectra (C. Kolczewski and K. Hermann, unpublished). This is in contrast to the situation at the $V_2O_5(010)$ surface where the rather simple geometric arrangement of the one, two, and threefold coordinated oxygen allows an immediate geometric interpretation of the different atom-derived core excitation spectra [40,41].

A comparison of the theoretical total and atom-derived spectra for the two different photon beam angles α yields differences due to the angular dependence of the transition probabilities of the different dipole excitations. This can be described analytically [40] by angle-resolved spectral intensities which are given by corresponding dipole transition matrix elements $m = (m_x, m_y, m_z)$ involving the initial core orbital φ_i and final excited state orbitals φ_f with

$$m = (m_x, m_y, m_z) = \langle \varphi_f | \mathrm{e} \cdot r | \varphi_i \rangle \,, \quad (1)$$

together with angular dependent factors describing the polarization direction of the incoming radiation. For the hexagonal structure of the $V_2O_3(0001)$ surface and the present photon beam geometry, the spectral intensities simplify to

$$\mathrm{I(E,\ \alpha)} = \chi \cdot \mathrm{E} \cdot \left\{ 1/2 \left[m_x^2 + m_y^2 \right] \cos^2\alpha + m_z^2 \sin^2\alpha \right\} \,, \quad (2)$$

where χ is a scaling factor, E is the excitation energy, and α is the angle of the photon beam with respect to the surface normal. Equation (2) can explain the angle variation in the O(3) and O(4) derived spectra (see Fig. 2) by the symmetry of the final excited state orbitals. For O(3) 1s excitation, the corresponding final state orbitals of the upper region of peak set I have sizeable components perpendicular to the surface such that their transition moments m_z are larger in absolute size than those parallel to the surface, m_x and m_y. As a result, the absorption intensity I(E, α) is small in the upper region of peak set I for $\alpha = 0^\circ$ but large for $\alpha = 70^\circ$. The situation is reversed for final state orbitals about the energetic center of peak set I where the orbital compositions lead to m_z values which are smaller in absolute size than m_x and m_y. The O(3) excitations near the lower edge of peak set I are characterized by dipole transition moments where all components, m_x, m_y, m_z, are of similar size. Based on Eq. (2), this can explain the weak angle dependence of the corresponding low-edge peak. For O(4) 1s excitation, the peak in the upper region of peak set I loses intensity with increasing angle α, while the peaks of the central and lower region gain intensity. However, the O(4) derived spectrum depends somewhat less on the angle α, which reflects the fact that the transition matrix elements m_x, m_y, m_z for the three dipole directions are similar in size. Equation (2) describes also the angular dependence of the spectral intensity of peak set II characterized by transitions from O 1s core to 3p resonances. However, the number of final state orbitals is too large to give a simple interpretation of the peak distribution in terms of specific transitions.

A comparison of the total theoretical O 1s excitation spectra for angles $\alpha = 0^\circ, 70^\circ$ with experimental NEXAFS spectra in Fig. 2 shows overall rather good agreement concerning peak positions as well as relative absorption intensities. This confirms that both types of oxygen, O(3) and O(4), present near the $V_2O_3(0001)$ surface contribute to the NEXAFS spectrum. Based on the theoretical spectra, the assignment of the split peak at about 533 eV in the experimental spectrum can be described for both angles α by electronic transitions originating at the O(3) and O(4) 1s orbitals. Here, O(3) derived transitions determine the full peak region while O(4) transitions are responsible for the high energy part. The experimental peak near 524 eV does not have a counterpart in the theoretical spectra. It originates from vanadium 2p core to 3d orbital excitations, which are not considered by our theory since they would require a treatment including spin-orbit coupling, which is neglected by the present approach. The experimental peak near 545 eV, which is characterized from the theoretical spectra by O 1s to 3p transitions at both O(3) and O(4) sites, is broadened and loses intensity if the photon beam angle α is varied from 70° to 0°. While the broadening is reproduced in theoretical spectrum, the intensity loss is not obvious and has to be studied in greater detail.

3.2 Vanadyl termination $O_tV'O$

The $O_tV'O$ termination of the $V_2O_3(0001)$ surface after oxygen exposure includes singly coordinated vanadyl oxygen O(1) at the surface in addition to the threefold and fourfold coordinated oxygen species, O(3) and O(4), of the V′OV termination described above (see Fig. 1b, c). Therefore, core excitations from three differently coordinated oxygen centers determine the angle-resolved NEXAFS spectrum. Figure 3 shows theoretical oxygen 1s NEXAFS spectra obtained from the $V_{11}O_{36}$ cluster calculations where two incidence directions of the incoming photon beam, $\alpha = 70^\circ, 0^\circ$, are considered as before. The figure includes for both angles α total theoretical O 1s excitation spectra as stoichiometry-weighted superpositions of O(1), O(3), and O(4) derived contributions together with the corresponding O(1), O(3), and O(4) components. These spectra are compared with recent experimental oxygen K edge NEXAFS spectra [19] obtained from differences of PYD and sample current mode measurements (top curve of each plot).

As for the V′OV termination (Fig. 2) the theoretical spectra of Fig. 3 can be described by two sets of peaks below (set I) and above the ionization threshold (set II) originating from specific oxygen 1s core excitations. Here, the O 1s ionization threshold near 537 eV, sketched in gray in Fig. 3, covers a somewhat larger energy range, 1.4 eV, than for the V′OV termination, which is explained by the additional O(1) species whose 1s IP differs from the IP values of O(3), O(4) by 0.9 eV. An analysis of the final state orbitals (C. Kolczewski and K. Hermann, unpublished) corresponding to peaks of set I between 529 eV and 533 eV shows that, analogous with the V′OV termination, all excitations refer to electronic transitions from O 1s to final state orbitals which are weakly antibonding combinations of oxygen 2p and vanadium 3d contributions. The amount of antibonding character depends on the direction of the 2p contribution of each oxygen center with respect to its vanadium neighbors with their 3d contributions and distinguishes between the excitation energies.

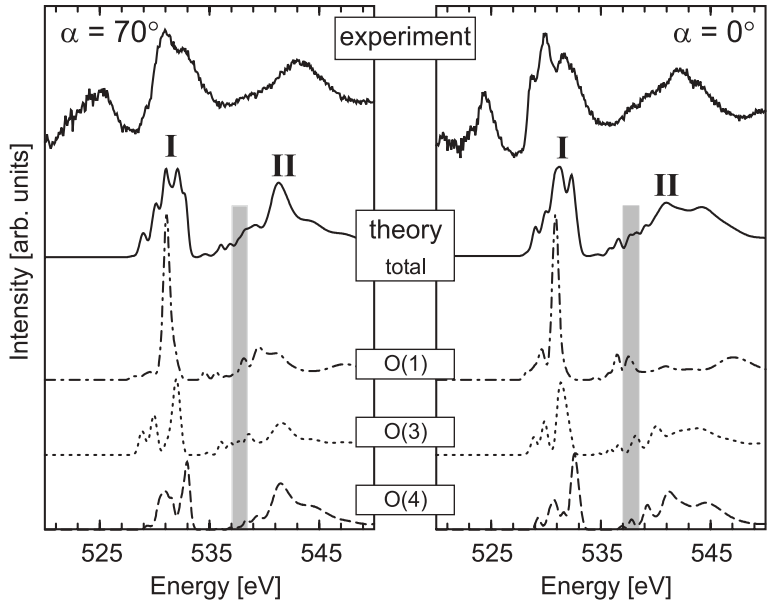

Fig. 3 Comparison of experimental angle-resolved O K edge NEXAFS spectra with theoretical O 1s core excitation spectra for two different angles of photon beam incidence, $\alpha = 0°$, 70°, at the $O_t V'O$ terminated $V_2O_3(0001)$ surface. For the evaluation of the experimental spectra, see text. The total theoretical spectra are decomposed into contributions from differently coordinated oxygen, O(1) (*dash-dotted*), O(3) (*dotted*), and O(4) (*dashed*). The gray line indicates corresponding oxygen 1s ionization potentials

The excitations of peak set II, which focuses at about 541 eV (i.e. above ionization threshold), are due to electronic transitions from O 1s to O 3p where, as before, the direction of the 3p functions together with the geometry of the local binding environment discriminates between the different excitations.

In addition to the total theoretical spectra, Fig. 3 contains atom-derived contributions due to singly, threefold, and fourfold coordinated oxygen, O(1) (dash-dotted curves), O(3) (dotted curves), and O(4) (dashed curves), respectively, which differ considerably in their intensity behavior. The O(1) derived contributions to peak set I are described, for both angles α, by one major peak at 531 eV with a smaller peak near 530 eV. The smaller low-energy peak represents several electronic transitions from O(1) 1s to final state orbitals which are mainly antibonding combinations of oxygen 2p (x, y) with vanadium 3d ($x^2 - y^2$, xy). Therefore, x and y components of the dipole transition matrix element, m_x and m_y (parallel to the surface), are much larger than m_z. As a consequence, the peak intensities according to Eq. (2) are expected to be larger for small angles α, which explains the behavior in Fig. 3. The large O(1) derived peak of set I at 531 eV originates from several excitations to final state orbitals which are antibonding combinations of oxygen 2p with vanadium 3d (xz, yz, z^2). Here, O 2p – V xz/yz combinations yield large transition moments m_x/m_y and smaller m_z while O 2p – V z^2 combinations lead to small m_x/m_y and larger m_z values. As a result, the two types of excitations yield absorption intensities according to Eq. (2) which complement each other such that the superimposed intensity depends only weakly on α. This can explain the close similarity of the O(1) derived peak at 531 eV for $\alpha = 0°$ and 70° in Fig. 3.

The energy ranges of both peak sets in Fig. 3 are larger for O(3) than for O(4) excitation and the O(3) derived set is shifted to lower energies with respect to that for O(4). In addition, the intensity distributions within peak set I differ between the two oxygen species. These differences can be explained analogous to the result for the $V'OV$ termination and originate from details of the local binding environment of the two types of oxygen as discussed before. In fact, the O(3) derived spectrum differs only slightly in peak set I between the $V'OV$ and $O_tV'O$ terminated $V_2O_3(0001)$ surfaces. This becomes obvious in a direct comparison of the theoretical $V'OV$ and $O_tV'O$ spectra for $\alpha = 0°$, given in Fig. 4. This figure demonstrates also that the fourfold coordinated oxygen O(4) yields almost identical spectra for the $V'OV$ and $O_tV'O$ termination. This is explained by the fact that the O(4) center is furthest away from the vanadyl oxygen O(1) which is added in the $O_tV'O$ compared to the $V'OV$ termination and is, therefore, affected least.

A comparison of the total theoretical O 1s excitation spectra for angles $\alpha = 0°$, 70° with experimental NEXAFS spectra for the vanadyl covered $V_2O_3(0001)$ surface [19] in Fig. 3 shows, as before, overall very good agreement concerning peak positions as well as relative absorption intensities. The experimental spectra contain, for both angles α, a structured peak at about 531 eV whose central feature at 531 eV can be assigned to electronic transitions originating at the O(1) species if information from the theoretical spectra is used. The intensity of this central feature depends only weakly on angle α, which is consistent with the theoretical findings discussed above. Analogous to the $V'OV$ termination, the experimental peak near 525 eV originates from vanadium 2p core to 3d

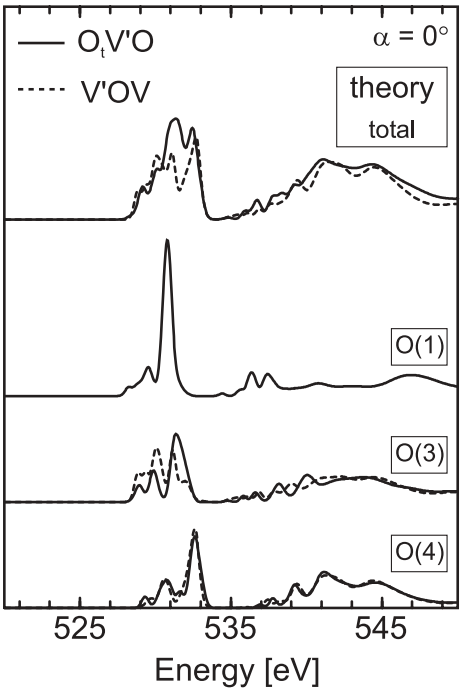

Fig. 4 Comparison of theoretical O 1s excitation spectra for the V′OV (dashed lines) and $O_tV'O$ (solid lines) surface terminations of the $V_2O_3(0001)$ surface for the photon beam incidence angle $\alpha = 0°$. The figure shows in addition to the total theoretical spectra their decompositions into contributions from differently coordinated oxygen, O(1), O(3), and O(4)

excitations, which are not considered by the present theory and, therefore, do not show up in the theoretical spectra for reasons mentioned before. The broad experimental peak near 543 eV is characterized from the theoretical spectra by O 1s to 3p transitions at both O(3) and O(4) sites while vanadyl O(1) contributions remain small.

4 Conclusions

The present ab initio DFT cluster studies on oxygen 1s core excitation of differently coordinated oxygen species at the $V_2O_3(0001)$ surface can give a clear picture of the underlying electronic mechanisms. The resulting theoretical core excitation spectra are in very good agreement with experimental angle-resolved oxygen K edge NEXAFS spectra for the clean (V′OV terminated) and oxygen covered ($O_tV'O$ terminated) single crystal surface [19]. The experimental spectra for the two terminations as well as for two different angles α of photon incidence exhibit three well-separated absorption regions each, of which two can be identified by the present theory as due to oxygen 1s core excitation involving differently coordinated oxygen species. First, the absorption region near 532 eV is characterized by O 1s core excitations to final state orbitals described as weakly antibonding combinations of oxygen 2p and vanadium 3d contributions. Here, the coordination of the corresponding oxygen species as well as its local binding geometry determines the angle-dependent absorption intensity. Second, the absorption region near 545 eV (above ionization threshold) can be assigned to electronic transitions from O 1s to 3p orbitals where, as before, the local binding geometry of the oxygen determines the transition probability and, thus, the absorption. Third, the absorption region near 525 eV originates from vanadium 2p core to 3d excitations, which cannot be considered by the present theory due to its neglect of spin-orbit coupling.

A decomposition of the theoretical spectra into contributions from differently coordinated oxygen can give further insight into details of the experimental NEXAFS spectra. For the half metal layer (V′OV) terminated $V_2O_3(0001)$, surface excitations from both three and fourfold coordinated oxygen are found to contribute to the spectrum (see Fig. 2). The split peak at about 533 eV in the experimental spectrum can be described for both angles α by O(3) derived transitions, with O(4) transition contributing to the high energy part. For the $O_tV'O$ terminated surface, the additional singly coordinated vanadyl O(1) species introduces new features in the experimental NEXAFS spectrum. Now, the energy region about 531 eV is characterized by three peaks (see Fig. 3) where, based on the theoretical data, the central peak is due to electronic transitions originating at the O(1) species. The intensity of this central feature depends only weakly on angle α both in the experimental and theoretical spectrum. Further, our theoretical analysis shows that contributions to the absorption intensity from O(3) core excitation are very similar for the V′OV and $O_tV'O$ terminations and O(4) core excitation contributions are virtually unchanged. This can be simply explained by the geometry of the two differently coordinated oxygen species. Altogether, the combination of the present theoretical spectra and experimental NEXAFS data for the $V_2O_3(0001)$ surface enables an identification of differently coordinated surface oxygen species in the system.

More detailed information on spectroscopic properties of the present system requires extended experimental NEXAFS studies for a full set of photon incidence and polarization angles in addition to microscopic surface structure data. Further, theoretical studies including other surface terminations as well as surface relaxation at the $V_2O_3(0001)$ surface have to be considered. Studies along these lines are currently under way (C. Kolczewski and K. Hermann, unpublished).

Acknowledgements This work was partly supported by Deutsche Forschungsgemeinschaft through Sonderforschungsbereich 546 "Transition Metal Oxide Aggregates". We thank Helmut Kuhlenbeck for fruitful discussions.

References

1. Kung HK (1989) Transition metal oxides: surface chemistry and catalysis. In: Delmon B, Yates JT (eds). Studies in surface sciences and catalysis. Elsevier, Amsterdam
2. Rao CNR, Raven B (1995) Transition metal oxides. VCH/ Weinheim, New York/Cambridge
3. Surnev S, Ramsey MG, Netzer FP (2003) Prog Surf Sci 73:117
4. Weckhuysen BM, Keller DE (2003) Catal Today 78:25

5. Grzybowska-Swierkosz B, Trifiro F, Vedrine JC (eds) (1997) Vanadia catalysts for selective oxidation of hydrocarbons and their derivatives. J Appl Catal 157:1, and references therein
6. Bond GC, Tahir SF (1991) Appl Catal 71:1
7. Kurtz RL, Henrich VE (1983) Phys Rev B 28:6699
8. Ezhov SY, Anisimov VI, Khomskii DI, Sawatzky GA (1999) Phys Rev Lett 83:4136
9. Catti M, Sandrone G (1997) Faraday Disc 189
10. Göring E, Schramme M, Müller O, Paulin H, Klemm M, denBoer ML, Horn S (1997) Physica B 230:996
11. Uozumi T, Okada K, Kotani A, Zimmermann R, Steiner P, Hufner S, Tezuka Y, Shin S (1997) J Electr Spectr Rel Phen 83:9
12. Kresse G, Surnev S, Schoiswohl J, Netzer FP (2004) Surf Sci 555:118
13. Preisinger M, Moosburger-Will J, Klemm M, Klimm S, Horn S (2004) Phys Rev B 69:
14. Henrich VE, Cox PA (1994) The surface science of metal oxides. University Press, Cambridge
15. Wang SB, Murata K, Hayakawa T, Hamakawa S, Suzuki K (2000) Appl Catal A 196:1
16. Wilde M, Seiferth O, Al-Shamery K, Freund HJ (1999) J Chem Phys 111:1158
17. Rohr F, Bäumer M, Freund HJ, Mejias JA, Staemmler V, Müller S, Hammer L, Heinz K (1997) Surf Sci 372:L291
18. Czekaj I, Hermann K, Witko M (2003) Surf Sci 525:33
19. Dupuis AC, Abu Haija M, Richter B, Kuhlenbeck H, Freund HJ (2003) Surf Sci 539:99
20. Goodenough JB (1971) In: Reiss H (ed) Progress in solid state chemistry, Vol 5, p 145
21. Dernier PD, Marezio M (1970) Phys Rev B 2:3771
22. Zachariasen WH (1998) Skrifter norske videnskaps—Akad. Oslo I. Mat.-Naturv. Klasse, No.4
23. Wyckoff RWG (1965) Crystal structures. Interscience Publishers, New York
24. Mattheiss LF (1994) J Phys Cond Matt 6:6477
25. Czekaj I, Witko M, Hermann K (2003) Surf Sci 525:46
26. Czekaj I, Hermann K, Witko M (2003) Surf Sci 545:85
27. The program package StoBe is a modified version of the DFT-LCGTO program package DeMon, originally developed by A. St.-Amant and D. Salahub (University of Montreal), with extensions by L.G.M. Pettersson and K. Hermann
28. Perdew JP, Burke K, Ernzerhof M (1996) Phys Rev Lett 77:3865
29. Hammer B, Hansen LB, Nørskov JK (1999) Phys Rev B 59:7413
30. Labanowski JK, Anzelm JW (1991) In: Density functional methods in chemistry. Springer, Berlin Heidelberg New York
31. Godbout N, Salahub DR, Andzelm J, Wimmer E (1992) Can J Chem 70:560
32. Kutzelnigg W, Fleischer U, Schindler M (1990) NMR-basic priniciples and progress. Springer, Berlin Heidelberg New York
33. The basis sets are taken from the StoBe basis set library
34. Pettersson LGM, Wahlgren U, Gropen O (1983) Chem Phys 80:7
35. Slater JC (1972) In: Loewdin PO (ed) Advances in quantum chemistry, Academic, New York
36. Slater JC, Johnson KH (1972) Phys Rev B 5:844
37. Ågren H, Carravetta V, Vahtras O, Pettersson LGM (1997) Theor Chem Acc 97:14
38. Kolczewski C, Püttner R, Plashkevych O, Ågren H, Staemmler V, Martins M, Snell G, Schlachter AS, Sant'Anna M, Kaindl G, Pettersson LGM (2001) J Chem Phys 115:6426
39. Triguero L, Pettersson LGM, Ågren H (1998) Phys Rev B 58:8097
40. Kolczewski C, Hermann K (2004) Surf Sci 552:98
41. Kolczewski C, Hermann K (2003) J Chem Phys 118:7599
42. Triguero L, Plashkevych O, Pettersson LGM, Ågren H (1999) J Electr Spectr Rel Phen 104:195.
43. Ogasawara H, Brena B, Nordlund D, Nyberg M, Pelmenschikov A, Pettersson LGM, Nilsson A (2002) Phys Rev Lett 89:276102